Optical properties of single diatom frustules revealed by confocal micro-spectroscopy

J. Romann,[1,*] J.-C. Valmalette,[2] A. Røyset,[3] M.-A. Einarsrud[1]

[1]*Norwegian University of Science and Technology (NTNU), NO-7491 Trondheim, Norway*
[2]*Université du Sud Toulon Var, IM2NP UMR 7334 CNRS, P.O. Box 20132, 83957 La Garde Cedex, France*
[3]*SINTEF Materials and Chemistry, NO-7465 Trondheim, Norway*
**Corresponding author: julien.romann@ntnu.no*

Received Month X, XXXX; revised Month X, XXXX; accepted Month X, XXXX; posted Month X, XXXX (Doc. ID XXXXX); published Month X, XXXX

Optical properties of single diatom frustule valves from two different *Coscinodiscus* species (*C. Wailesii* and *C. Centralis*) are studied by transmission confocal hyperspectral imaging and numerical calculations. Light convergence, concentration and trapping effects are observed and depend on both the wavelength and the valve orientation. These effects seem to occur independently of the incident light angle. From our results, a wavelength dependent multifocal lens behavior can be explained by light diffraction related to the radial symmetry of the multi-scaled 3D nanostructure. © 2014 Optical Society of America

OCIS Codes: (160.1435) Biomaterials, (080.3630) Optical materials, (080.3630) Lenses, (160.5298) Photonic crystals, (230.7370) Waveguides, (300.6550) Spectroscopy, visible.
http://dx.doi.org/10.1364/OL.99.099999

Biological organisms relying on sunlight for survival have evolved for several millions of years to optimize their light harvesting, manipulation or conversion efficiency. For many of these organisms, this evolution process involves the building of complex nano-scaled biological structures with special optical properties. One of the most noteworthy examples of optical bio-nanostructures is the complex nanoporous shell (frustule) produced by diatoms, a major group of phytoplankton found in both marine and freshwater environments [1]. Diatoms have recently attracted significant attention for potential applications in nanotechnology [1-11], especially regarding the optical properties of the bio-silica frustules they synthesize [12-19]. Among thousands of different species classified according to the geometry of the frustules, several diatom species have been subject to studies related to their remarkable optical behavior. Photonic crystal properties have been anticipated for frustules of *Coscinodiscus granii* diatoms [12] and a light focusing effect has been measured for *Coscinodiscus wailesii* diatom frustules [14]. A dependence between the spatial distribution of light transmitted through a single Coscinodiscus wailesii frustule and the wavelength has also been reported [18]. Although neither providing visualization nor thorough transmission spectra analysis, this study reported interesting computational results suggesting light confinements effects below the diffraction limit of a lens with the dimensions of the modeled frustule.

In this work, we use bidimensional (2D) hyperspectral transmission mapping measurements to study the optical properties of single frustules of *Coscinodiscus centralis* (CC) and *Coscinodiscus wailesii* (CW) diatoms. Our aim is to provide a new insight on these properties using direct visualization of the light distribution after transmission through diatom frustules with different structures.

Diatom frustules of the Coscinodiscus genus consist of two valves and girdle bands joining the two facing valves. The CC diatoms were collected in the Trondheim fjord (Norway, 63°29'N, 10°15'E) and the CW diatoms were grown in a lab facility. All frustules were cleaned with a hydrogen peroxide aqueous solution to obtain separated valves and girdle bands. Single valves were studied in ambient air on a quartz substrate using a custom optical setup involving a confocal micro-spectrometer (Fig. 1). In this setup, a tungsten halogen light source illuminates the sample from below using an optical fiber with a diameter of 1000 µm. A motorized stage allows bidirectional motion of the sample in the plane of the substrate (XY plane). The transmitted light is collected by a 100x objective (NA 0.9) mounted on a vertically (Z axis) moving motorized stage. The objective is always aligned with the central axis of the optical fiber, where the incident beam is assumed to be

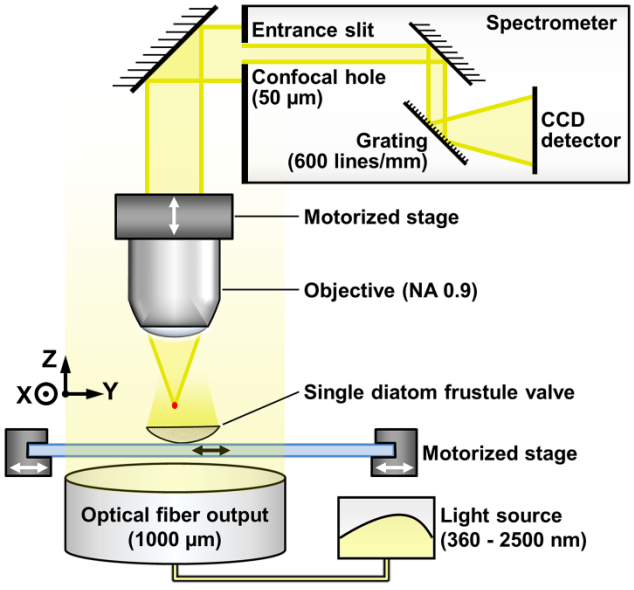

Fig. 1. Experimental setup.

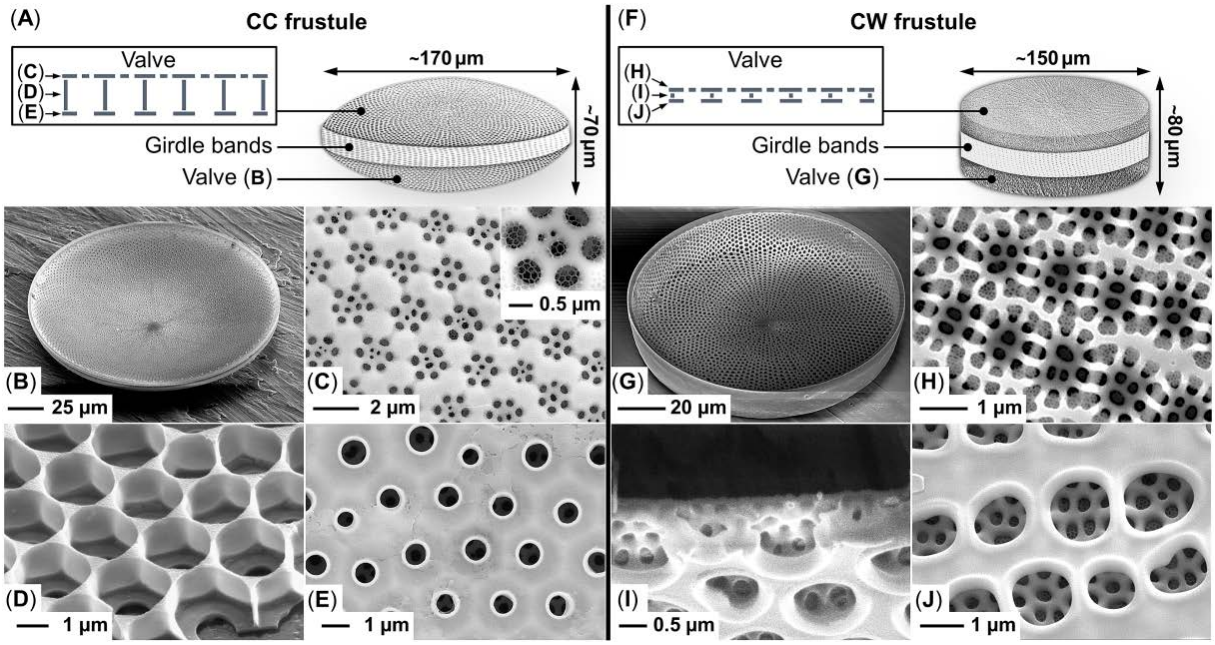

Fig. 2. (A) Scheme of a CC frustule; SEM images of: (B) a CC valve, (C) the CC *cribrum*, (D) the CC *areola* after stripping of the *cribrum*, (E) the CC *foramen*; (F) scheme of a CW frustule; SEM images of: (G) a CW valve, (H) the CW *cribrum*, (I) a cross-section view of a CW valve; (J) the CW *foramen*.

parallel below the frustule. The collected light is directed through a confocal hole (50 µm), and dispersed on a CCD detector by a grating. Maps acquired along the XY and the YZ planes are called XY and YZ maps respectively. Hyperspectral maps (hypermaps) show the spatial distribution of transmission spectra, which were acquired from 625 to 675 nm. The greyscale in the hypermaps corresponds to the integrated intensity of each transmission spectrum over this wavelength range. Monochromatic maps (λ-maps), showing the spatial distribution of transmitted light intensity at a fixed wavelength (λ), were extracted from each hypermap. The greyscale in the λ-maps corresponds to the light intensity at the chosen wavelength.

The complex porous structure of both studied valves (CC and CW) consists of two symmetries: a radial symmetry at the scale of the whole valve (the pores are arranged radially around the valve center), and a hexagonal symmetry at the scale of a few porous patterns. The CC valve (Fig. 2(A), 2(B)) can be considered as the superposition of three layers. The external layer (cribrum) shows a porous array of flower-like patterns (Fig. 2(C)). Beneath the cribrum is the areola, a honeycomb structure of walls perpendicular to the cribrum (Fig. 2(D)). Each pattern of the cribrum is centered above a cavity defined by the areola. The internal layer (foramen) shows an array of circular pores (Fig. 2(E)), each centered with both a cavity of the areola and a pattern of the cribrum. The CW valve (Fig. 2(F), 2(G)) has the same overall structure as a CC valve, but with some differences. Whereas a CC valve has a lens-like shape (Fig. 2(B)), the shape of a CW valve is more like a petri-dish (Fig. 2(G)). The cribrum (Fig. 2(H)) has a more complex porous structure with higher porosity. The most striking difference lies in the areola, which is almost nonexistent (Fig. 2(I)). Finally, the pores of the foramen (Fig. 2(J)) appear less circular than for the CC valve.

Numerical simulations of periodic structures mimicking the frustule structure were carried out with the diffraction calculation software GdCalc from KJ Innovations. The structural parameters were estimated from SEM images of CC valves as following: hole distance d = 2.2 µm, hole radius 0.5 µm, areola height 2.2 µm and thickness of areola walls, cribrum and foramen were 0.2 µm. The flower pattern of the cribrum layer was modeled as 0.5 µm radius holes with equal proportions of air and silica (effective medium). The intensity at the confocal volume was calculated from the contribution of a large number of small periodic areas arranged in the radial symmetry.

The experimental YZ hypermaps shown in Fig. 3 compare the optical properties of CC and CW single valves. These maps reveal the intensity distribution of light transmitted through the valves oriented with their cribrum layers facing the light source. An area of high light intensity is detected above the centers of both valves. In the case of the CC valve, this area spreads from about 50 µm to 170 µm above the valve. For the CW valve, this high intensity area spreads right from the foramen to about 30 µm above the valve. These high light intensity areas correspond to a significant light concentration effect, which seems to arise from a global convergence phenomenon. This effect can be related to the focusing effect previously measured for the CW valves [14], but the location of the light concentration area and the shape of the CW valve are not consistent with classic lens-induced convergence. It is very unlikely that the difference in global shape between the CC valve and the CW valve could be responsible for the observed optical differences as CC valves of different curvatures show very similar transmission maps. This necessarily implies a strong influence of the porous nanostructure on the resulting optical properties. The comparison of the two hypermaps also suggests that the two light concentration effects could emerge from two different phenomena. We will later show that the

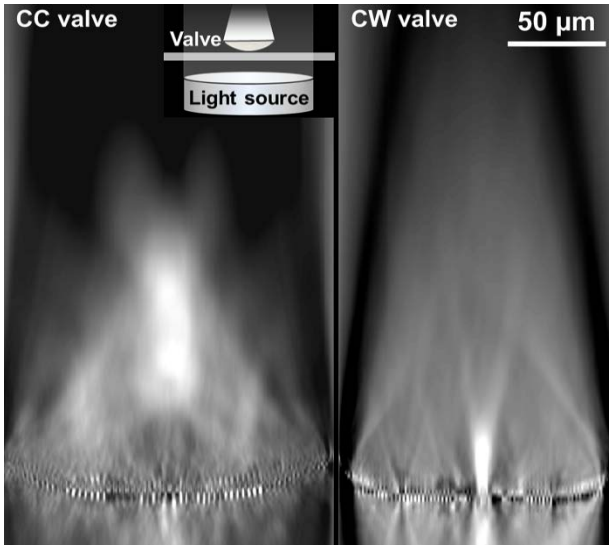

Fig. 3. YZ hyper-maps of single CC and CW valves. The scheme shows the illumination configuration and the scale bar is the same for both maps.

observation for the CC valve can be explained by multiple diffraction phenomena. The origin of the transmission observed for the CW valve is uncertain, but could arise from a waveguide phenomenon as the distance between the cribrum and foramen layers is close to the investigated wavelength range. The next results will be only focused on the CC valve.

The influences of the incident light angle and the orientation of a CC valve on the transmitted intensity distribution are also studied using hypermaps (Fig. 4). For a valve oriented with its cribrum facing a normal incident light (Fig. 4(A)), the intensity is symmetrically distributed around the symmetry axis of the valve (S axis).

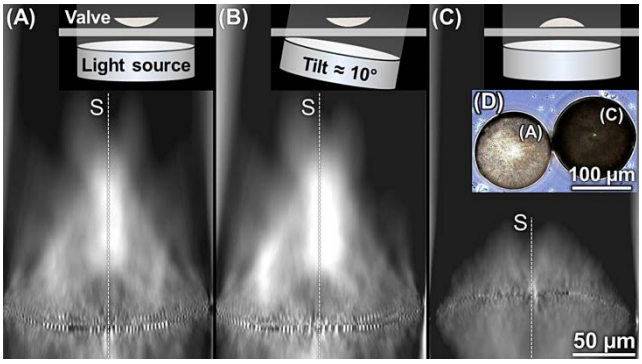

Fig. 4. YZ hyper-maps ((A), (B), (C)) and transmission optical microscopy image ((D)) of CC valves; (A) *cribrum* faces a normal incident light; (B) *cribrum* faces a tilted incident light; (C) *foramen* faces a normal incident light. The schemes show the illumination configuration. The symmetry axis of the valve (S) is indicated by a vertical dotted line. The scale bar is the same for all hyper-maps.

angle of the incident light. The second effect is an increase of the light concentration localized along the S axis. The third effect is a disruption in the light distribution symmetry, as the measured intensities are globally higher on the side from which the light is coming. These three effects cannot be explained by classic lens-induced convergence. When the incident light is normal to a valve having its foramen oriented towards the light source (Fig. 4(C)), no light concentration effect is observed. The global intensity of the transmitted light is considerably reduced, becoming negligible from about 50 µm above the valve. This effect is also observed in transmission optical microscopy as single valves appear darker when their foramen is oriented towards the light source (Fig. 4(D)).

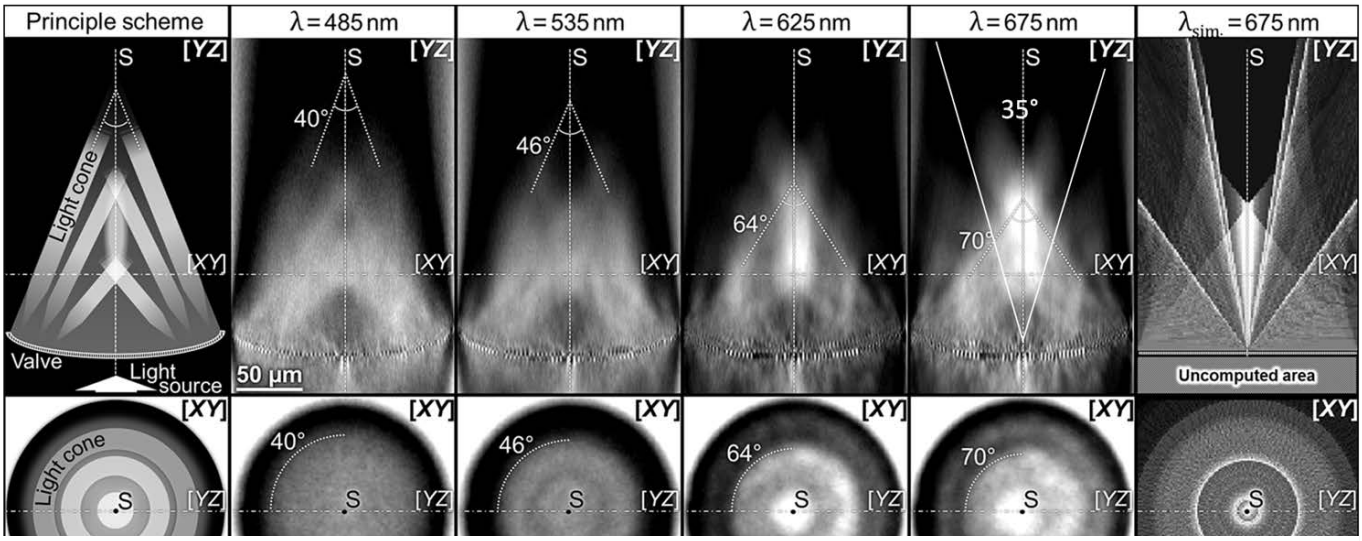

Fig. 5. YZ (top maps), corresponding XY (bottom maps) λ-maps of a CC valve, principle scheme of the observed maps (left column) and simulation maps from the modeled CC valve structure (right column). The symmetry axis of the valve (S) is indicated by a vertical dotted line (top) and a black dot (bottom). The alternate mapping planes are indicated by horizontal dash-dot lines. A light cone is indicated by dotted lines in the λ-maps. The scale bar is the same for all maps and the principle scheme.

surprisingly, the direction of the transmitted light is unchanged, suggesting that it may be independent of the

asymmetric optical properties caused by the substantial difference in the porous structure between the cribrum and

the foramen. If not transmitted, much of the light must therefore be reflected back towards the light source.

In Fig. 5 are shown eight experimental λ-maps of a CC valve at λ = 485, 535, 625 and 675 nm, respectively. For each wavelength, both an YZ map and a corresponding XY map are displayed. A simulated λ-map is also displayed for a wavelength of λ = 675 nm. In addition, a principle scheme helps understanding what is observed in the λ-maps. It becomes clearer here that the transmitted light is observed as the resulting combination of multiple light convergence cones centered on the symmetry axis of the valve (S axis). Our 2D hyperspectral experiments and simulation results clarify the light convergence angle increase with the wavelength previously reported on CW valve [18]. Indeed, the simulation result in Fig. 5 shows that the strong light focusing along the S axis for 675 nm light can be explained by light diffraction. The two main contributions are the (0,1) diffraction oriented ±30° relative to the radial direction and the (1,2) diffraction oriented along the radial direction. Both have a 60° symmetry and are caused by periodicities of d*cos(π/6) and d/2 respectively, causing diffraction angles of 20.75° and 37.85°, respectively at 675 nm. The radial focusing caused by (1,2) diffraction is the main contributor to the strong light concentration at the S axis about 100 μm above the valve in the numerical map. This corresponds to a diffraction angle of 37° from the edge of the frustule, corresponding well with the experimentally observed light cone of ±35°. In the numerical XY map, the light intensity at the S axis is caused by the (1,2) diffraction, while the focused ring with radius ~15 μm is caused by (0,1) diffraction. When the wavelength is reduced, numerically computed maps change due to two main effects. Firstly the diffraction angles are reduced, secondly the relative contribution from (0.1) and (1,2) diffraction are is altered. At 625 and 675 nm the (1,2) diffraction are stronger than the (0,1) diffraction, while the opposite is the case at 485 and 535 nm. This can explain why the focusing effect is much stronger at 625 and 675 nm. Simulations also show that the hexagonal walls are the main contributor to the (1,2) diffraction. These walls are almost absent in the CW frustules, which therefore has a light concentration dominated by (0,1) diffraction at all wavelengths. There are several observed differences between the experimental and the numerical maps. These differences may be caused by local variations of structural parameters and the frustule curvature, both of which the simulation does not take into account. Despite these inaccuracies, the numerical results based on diffraction can explain many of the observed phenomena observed at different wavelengths and with different structures.

This work enabled the direct observation of remarkable optical properties at the scale of the frustule porous structure. Both CC and CW frustule valves induce a light concentration phenomenon comparable to a focusing effect. The light concentration and trapping phenomena depending on the valve orientation and the special optical behavior observed when tilting the incident light are strong indicators of optical waveguide properties. Multiple convergence light cones emerge from a single valve making it similar to a multifocal lens can be explained by diffraction. These optical effects may explain the light trapping mechanism of diatoms and could inspire new ways of designing future optical nanostructures.

This work was supported by the Research Council of Norway (contract #10358700). We acknowledge Prof. Gabriella Tranell for leading this research project, Dr. Matilde Chauton for growing and extracting the diatom frustules and Marius Vebner for his contribution to obtain the SEM pictures presented in this work.

References

1. W. Yang, P. J. Lopez, and G. Rosengarten, Analyst **136**, 42-53 (2011)
2. J. Parkinson, and R. Gordon, Nanotechnol. **17**, 190-196 (1999)
3. D. Losic, J. G. Mitchell, and N. H. Voelcker, New J. Chem. **30**, 908-914 (2006)
4. M. Sumper, and E. Brunner, Adv. Funct. Mater. **16**, 17-26 (2006)
5. D. Losic, K. Short, J. G. Mitchell, R. Lal, and N. H. Voelcker, Langmuir **23**, 5014-5021 (2007)
6. R. Gordon, D. Losic, M. A. Tiffany, S. S. Nagy, and F. A. S. Sterrenburg, Trends Biotechnol. **27**(2), 116 (2008)
7. N. Kröger, and N. Poulsen, Annu. Rev. Genet. **42**, 83-107 (2008)
8. H. E. Townley, A. R. Parker, and H. White-Cooper, Adv. Funct. Mater. **18**, 369-374 (2008)
9. D. Losic, J. G. Mitchell, and N. H. Voelcker, Adv. Mater. **21**, 2947 (2009)
10. Y. Yu, J. Addai-Mensah, and D. Losic, Langmuir **26**(17), 14068-14072 (2010)
11. N. Nassif, and J. Livage, Chem. Soc. Rev. **40**, 849-859 (2011)
12. T. Fuhrmann, S. Landwehr, M. El Rharbi-Kucki, and M. Sumper, Appl. Phys. B **78**, 257 (2004)
13. L. De Stefano, M. De Stefano, I. Rea, L. Moretti, A. Bismuto, P. Maddalena, and I. Rendina, Proc. SPIE **5925**, 0277-786X/05/$15 (2005)
14. L. De Stefano, I. Rea, I. Rendina, M. De Stefano, and L. Moretti, Opt. Express **15**(26), 18082 (2007)
15. A. R. Parker, and H. E. Townley, Nat. Nanotechnol. **2** (June 2007), 347-353 (2007)
16. L. De Stefano, L. Rotiroti, M. De Stefano, A. Lamberti, S. Lettieri, A. Setaro, and P. Maddalena, Biosens. Bioelectron. **24**, 1580 (2008)
17. S. Yamanaka, R. Yano, H. Usami, N. Hayashida, M. Ohgushi, H. Takeda, and K. Yoshino, J. Appl. Phys. **103**, 074701 (2008)
18. E. De Tommasi, I. Rea, V. Mocella, L. Moretti, M. De Stefano, I. Rendina, and L. De Stefano, Opt. Express **18**(12), 12203-12212 (2010)
19. M. P. Andrews, A. Hajiaboli, J. Hiltz, T. Gonzalez, G. Singh, and R. B. Lennox, Proc. SPIE **7946**, 79461S (2011)
20. C. S. French, Arch. Mikrobiol. **59**, 93-103 (1967)
21. M. Zapata, F. Rodriguez, and J. L. Garrido, Mar. Ecol. Prog. Ser. **195**, 29-45 (2000)
22. T. Fujiki, and S. Taguchi, J. Plankton Res. **24**(9), 859-874 (2002)
23. P. Yao, Z. Yu, C. Deng, S. Liu, and Y. Zhen, Chin. J. Oceanol. Limnol. **29**(5), 1075-1085 (2011)

Full references list

1. W. Yang, P. J. Lopez, and G. Rosengarten, "Diatoms: self-assembled silica nanostructures, and templates for bio/chemical sensors and biomimetic membranes", Analyst **136**, 42-53 (2011)
2. J. Parkinson, and R. Gordon, "Beyond micromachining: the potential of diatoms", Nanotechnol. **17**, 190-196 (1999)
3. D. Losic, J. G. Mitchell, and N. H. Voelcker, "Fabrication of gold nanostructures by templating from porous diatom frustules", New J. Chem. **30**, 908-914 (2006)
4. M. Sumper, and E. Brunner, "Learning from diatoms: nature's tools for the production of nanostructured silica", Adv. Funct. Mater. **16**, 17-26 (2006)
5. D. Losic, K. Short, J. G. Mitchell, R. Lal, and N. H. Voelcker, "AFM nanoindentations of diatom biosilica surfaces", Langmuir **23**, 5014-5021 (2007)
6. R. Gordon, D. Losic, M. A. Tiffany, S. S. Nagy, and F. A. S. Sterrenburg, "The glass menagerie: diatoms for novel applications in nanotechnology", Trends Biotechnol. **27**(2), 116 (2008)
7. N. Kröger, and N. Poulsen, "Diatoms - from cell wall biogenesis to nanotechnology", Annu. Rev. Genet. **42**, 83-107 (2008)
8. H. E. Townley, A. R. Parker, and H. White-Cooper, "Exploitation of diatom frustules for nanotechnology: tethering active biomolecules", Adv. Funct. Mater. **18**, 369-374 (2008)
9. D. Losic, J. G. Mitchell, and N. H. Voelcker, "Diatomaceous lessons in nanotechnology and advanced materials", Adv. Mater. **21**, 2947 (2009)
10. Y. Yu, J. Addai-Mensah, and D. Losic, "Synthesis of self-supporting gold microstructures with three-dimensional morphologies by direct replication of diatom templates", Langmuir **26**(17), 14068-14072 (2010)
11. N. Nassif, and J. Livage, "From diatoms to silica-based biohybrids", Chem. Soc. Rev. **40**, 849-859 (2011)
12. T. Fuhrmann, S. Landwehr, M. El Rharbi-Kucki, and M. Sumper, "Diatoms as living photonic crystals", Appl. Phys. B **78**, 257 (2004)
13. L. De Stefano, M. De Stefano, I. Rea, L. Moretti, A. Bismuto, P. Maddalena, and I. Rendina, "Optical characterization of biological nano-porous silica structures", Proc. SPIE **5925**, 0277-786X/05/$15 (2005)
14. L. De Stefano, I. Rea, I. Rendina, M. De Stefano, and L. Moretti, "Lensless light focusing with the centric marine diatom Coscinodiscus wailesii", Opt. Express **15**(26), 18082 (2007)
15. A. R. Parker, and H. E. Townley, "Biomimetics of photonic nanostructures", Nat. Nanotechnol. **2** (June 2007), 347-353 (2007)
16. L. De Stefano, L. Rotiroti, M. De Stefano, A. Lamberti, S. Lettieri, A. Setaro, and P. Maddalena, "Marine diatoms as optical biosensors", Biosens. Bioelectron. **24**, 1580 (2008)
17. S. Yamanaka, R. Yano, H. Usami, N. Hayashida, M. Ohgushi, H. Takeda, and K. Yoshino, "Optical properties of diatom silica frustule with special reference to blue light", J. Appl. Phys. **103**, 074701 (2008)
18. E. De Tommasi, I. Rea, V. Mocella, L. Moretti, M. De Stefano, I. Rendina, and L. De Stefano, "Multi-wavelength study of light transmitted through a single marine centric diatom", Opt. Express **18**(12), 12203-12212 (2010)
19. M. P. Andrews, A. Hajiaboli, J. Hiltz, T. Gonzalez, G. Singh, and R. B. Lennox, "Nanoplasmonic photonic crystal diatoms and phytoliths", Proc. SPIE **7946**, 79461S (2011)
20. C. S. French, "Changes with age in the absorption spectrum of chlorophyll a in a diatom", Arch. Mikrobiol. **59**, 93-103 (1967)
21. M. Zapata, F. Rodriguez, and J. L. Garrido, "Separation of chlorophylls and carotenoids from marine phytoplankton: a new HPLC method using a reversed phase C8 column and pyridine-containing mobile phases", Mar. Ecol. Prog. Ser. **195**, 29-45 (2000)
22. T. Fujiki, and S. Taguchi, "Variability in chlorophyll a specific absorption coefficient in marine phytoplankton as a function of cell size and irradiance", J. Plankton Res. **24**(9), 859-874 (2002)
23. P. Yao, Z. Yu, C. Deng, S. Liu, and Y. Zhen, "Classification of marine diatoms using pigment ratio suites", Chin. J. Oceanol. Limnol. **29**(5), 1075-1085 (2011)